Available online at www.sciencedirect.com
SCIENCE DIRECT
ELSEVIER
Polymer 46 (2005) 3056–3068
polymer
www.elsevier.com/locate/polymer

The role of crystalline phase on fracture and microstructure evolution of polytetrafluoroethylene (PTFE)

Eric N. Brown[a,*], Dana M. Dattelbaum[b]

[a]Materials Science and Technology Division, Los Alamos National Laboratory, MS E544, Los Alamos, NM 87545, USA
[b]Dynamic Experimentation and Materials Science and Technology Divisions, Los Alamos National Laboratory, MS P952, Los Alamos, NM 87545, USA

Received 16 November 2004; received in revised form 14 January 2005; accepted 20 January 2005
Available online 9 March 2005

Abstract

Polytetrafluoroethylene (PTFE) is a semi-crystalline polymer, which has been employed in a range of engineering applications due to its extremely low coefficient of friction, resistance to corrosion, and excellent electrical insulation properties. Despite failure-sensitive applications such as surgical implants, aerospace components, motor seals, and barriers for hazardous chemicals, the mechanisms of crack propagation in PTFE have received limited coverage in the literature. Moreover, PTFE exhibits complex crystalline phase behavior that includes four well-characterized phases with both local and long range order. Three crystalline structures (phases II, IV, and I) are observed at atmospheric pressure with transitions between them occurring at 19 and 30 °C. This observation provides a unique opportunity for investigation of the effects of a polymers crystalline phase on fracture and microstructure evolution. Moreover, due to the presence of three unique ambient pressure phases near room temperature, it is essential to develop an understanding of the effects of temperature-induced phase transitions on fracture mechanisms of PTFE to prevent failure over the normal range of operating temperatures. In this work, we present values for the *J*-integral fracture toughness of PTFE for a range of temperatures and loading rates employing the single specimen normalization technique. Crack propagation in PTFE is found to be strongly phase dependent with a brittle-to-ductile transition in the crack propagation behavior associated with the two room temperature phase transitions. Increases in fracture toughness are shown to result from the onset of stable fibril formation bridging the crack plane and increased plastic deformation. The stability of drawing fibrils is primarily determined by temperature and crystalline phase with additional dependence on loading rate and microstructure anisotropy. [LAUR-05-0004]

Keywords: Polytetrafluoroethylene (PTFE); Phase transformation; *J*-integral compact tension (CT)

1. Introduction

Compared with other polymers, those containing fluorine present several advantages for load-bearing structural components including higher strength at elevated temperatures and higher toughness at lowered temperatures [1]. Failure sensitive applications of fluorocarbon polymers include surgical implants, aerospace components, motor seals, and barriers for hazardous chemicals. The most widely used fluorocarbon polymer for engineering applications is polytetrafluoroethylene (PTFE), $-(CF_2)_n-$, which possesses a combination of desirable chemical and physical properties including excellent high temperature stability [2], chemical resistance [3], dielectric properties [4] and extremely low coefficient of friction [5]. Polytetrafluoroethylene is semi-crystalline in nature, with its linear chains adopting complicated phases within crystalline domains near room temperature and ambient pressure. The mechanical characteristics of PTFE, including fracture and damage evolution, exhibit significant dependence on subtle changes in the polymer structure. Due to the presence of three unique phases near room temperature and ambient pressure, crack propagation in PTFE is strongly dependent on the crystalline phase transitions during standard operating conditions [6]. The typical range of temperatures a structural material is anticipated to encounter is −40 to 40 °C. This paper presents a systematic study of fracture and microstructure

* Corresponding author. Tel.: +1 505 667 0799; fax: +1 505 667 2185.
E-mail address: en_brown@lanl.gov (E.N. Brown).

0032-3861/$ - see front matter © 2005 Elsevier Ltd. All rights reserved.
doi:10.1016/j.polymer.2005.01.061

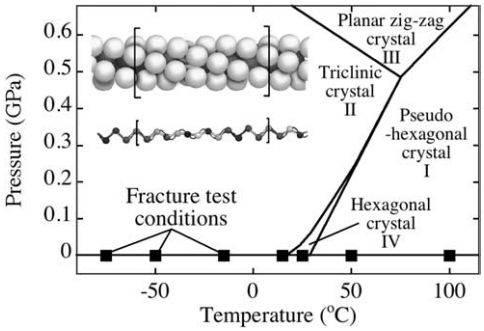

Fig. 1. Temperature–pressure phase diagram for PTFE and crystalline structure of PTFE in phase II [8].

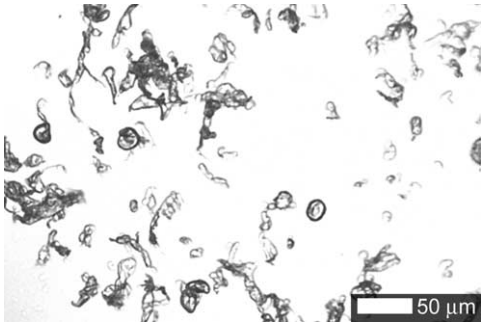

Fig. 2. Optical micrograph of the structure of PTFE 7C molding powder.

evolution of PTFE relating the effects of temperature induced crystalline phase on fracture mechanisms for pedigreed Teflon®[1] PTFE 7C polymer, i.e. polymer samples where the chemistry and manufacturing method were carefully controlled and documented.

The phase behavior of PTFE, as first reported by Bunn and Howells in 1954 [7] and shown in Fig. 1 [8,9], is particularly interesting with two atmospheric pressure crystalline transitions at 19 °C [7] and 30 °C [1]. Substantial molecular motion within the crystal is observed well below the melting point (328 °C in the billets used in this investigation and 341 °C in the molding powder), with α and γ glass like transitions at −80 and 126 °C [10]. The first-order transition at 19 °C between phases II and IV is an unraveling in the helical conformation from a well-ordered triclinic structure with 13 atoms/180° turn (inset in Fig. 1) [1,11] to a partially ordered hexagonal phase with 15 atoms/turn [1,8,12]. Further rotational disordering and untwisting of the helices occurs above 30 °C giving way to phase I to form a pseudohexagonal structure with dynamic conformational disorder and long-range positional and orientational order [1,2]. There also exists a fourth phase at high pressure, which is not studied in the current investigation.

Despite an extensive body of work in the literature investigating aspects of the chemical structure of PTFE, such as the crystalline phase transitions and the percent crystallinity, these studies have focused on virgin, as manufactured—pressed and sintered—material. Conversely, most studies of the mechanical behavior of PTFE have either focused on a single temperature [13,14] or disregarded the occurrence of phase transitions over the temperature range investigated [15–19]. Notable exceptions include work by McCrum [20], Vincent [21] and Kisbenyi et al. [22] correlating changes of the modulus and loss factor with phase transitions. Moreover, the mechanical and chemical characteristics of PTFE are strongly dependent on the grade of molding powder and method of processing used to manufacture the polymer, yet the majority of work in the literature reports on generic samples tested without sufficient description of the polymer's pedigree. To illustrate the process dependent variation, the crystallinity of PTFE molding powder resin ranges from 93–98% and is subsequently reduced to 40–80% crystallinity in the final product due the melting and recrystallization that occur during sintering and cooling of the polymer [22–24].

Due to the non-linear mechanical behavior of PTFE (discussed at length by Rae and Brown [25]), the fracture behavior cannot be captured by linear-elastic fracture mechanics (LEFM). Therefore, a *J*-integral analysis has been performed to measure the non-linear elastic–plastic strain energy fracture toughness, J_{IC}, using the single compact tension (CT) normalization technique outlined in ASTM E1820. The added complexity of experimental measurements for non-linear fracture behavior has lead to limited investigation of the fracture behavior of PTFE in the literature. Vincent et al. [21] and Kisbenyi et al. [22] reported linear-elastic strain energy release rate, G_C, values for fracture of PTFE, acquired from a Charpy impact test using a notched bar specimen. They subsequently correlated fracture toughness with tan δ loss data from dynamic mechanical analysis (DMA). This analysis subsequently includes two major limitations; (1) the analysis assumes the fracture behavior to be elastic at all temperatures and (2) the kinetic energy imparted into the sample must be removed from the calculated values of G_C necessitating several correction methods. However, Kisbenyi et al. [22] report several significant characteristics of PTFE fracture, including dependence on rate and crystallinity, and distinct transitions in the energy required to propagate a crack on associated with the crystalline phase transitions. Joyce has recently reported on low temperature fracture of PTFE [17,18] and metal filled PTFE [19], and Aglan et al. [26] have presented on the room temperature fatigue behavior of filled PTFE. In these cases, the effect of crystalline phase transitions on fracture behavior has been neglected.

2. Experimental procedure

2.1. Materials and sample preparation

The pedigreed PTFE polymer investigated in the current

[1] Teflon® is a registered trademark of DuPont.

Table 1
Mass fraction crystallinity values for PTFE 7C by standard methods [28]

He-pycnometry density, kg/m^3	Immersion density (kg/m^3)	MDSC crystallinity (%)	Density crystallinity (%)	IR crystallinity (%)	WAXS crystallinity (%)
2168.9±0.1	2169.6±0.1	38±1	48±1	73±10 (7A)	69±2

work was manufactured from PTFE 7C molding powder that was acquired from DuPont [27]. The molding powder, shown in Fig. 2, has an aspect ratio significantly larger than most PTFE molding powders (as high as 20:1) and a crystallinity of 87% (by density) [6]. The near spherical geometry of most PTFE molding powder grades, such as PTFE 7A produces a random orientation of particles and a uniform microstructure. The high aspect ratio PTFE 7C molding powder on the other hand exhibits beneficial properties for manufacturing PTFE matrix composites, but leads to particle orientation during the pressing process, i.e. texture. Billets measuring $600\times600\times65$ mm^3 were pressed and sintered by Balfor Industries (NY) following ASTM D-4894-98a resulting in crystallinity a of approximately 48% (by density) [28]. An initial pressure of 3.45 MPa was applied, which was ramped to 34.5 MPa at 3–5 MPa/min. The pressed billet was sintered by an accurately controlled thermal profile; 36 °C/h to 300 °C, hold for 6 h, 36 °C/h to 357 °C, hold for 6 h, cooled to room temperature at 36 °C/h. Values of crystallinity and density for the pedigreed PTFE 7C are provided in Table 1. A review of methods for measuring crystallinity in PTFE has been presented by Lehnert et al. [29] including a discussion of variability in results. The temperature (−50 to 150 °C) and rate (5×10^{-5}–8×10^{2}/s) dependence of the tensile response for this pedigreed PTFE 7C have previously been reported by Rae and Brown [25]. Joyce [17] has reported the tensile behavior of PTFE 7C (of unreported processing) for temperatures down −75 °C. Rae and Dattelbaum [28] have previously investigated the compressive stress–strain behavior of pedigreed PTFE 7C and provided an extensive discussion of the challenges associated with evaluating crystallinity. The initial tangent moduli and 2% offset yield stress values used in this work are given in Table 2. As discussed in Rae and Brown [25], variability in the data arose from a combination of data analysis and sample-to-sample variation. Errors associate with assigning the tangent modulus at small strains introduced the largest loss in accuracy, with up to 7.5% error in the tangent modulus and associated 2.5% error in the yield stress. Sample-to-sample variability was determined to be small: less than 3% error in the tangent modulus and 2.5% error in the yield stress (for three samples at 25 °C, 0.005 s^{-1}).

Table 2
Mechanical properties for PTFE 7C in tension as a function of temperature

Temperature (°C)	Modulus (GPa)	Yield stress (MPa)
100	0.29[a]	3.3[a]
50	0.49[a]	6.0[a]
25	0.58[a]	9.2[a]
15	0.97[a]	13.2[a]
−15	1.59[a]	20.6[a]
−50	3.21[a]	27.8[a]
−73	3.19[b]	43.8[b]

[a] From [25], at constant true strain rate of 5×10^{-3}/s.
[b] From [17], at constant engineering strain rate of 2.5×10^{-5}/s.

Specimens were machined from the pressed and sintered billets of pedigreed PTFE 7C while ensuring a nominal temperature rise to prevent changes in the material crystallinity. Two sets of fracture specimens were machined such that the crack propagation would either occur parallel (∥) to or perpendicular (⊥) to the pressing direction, as illustrated in Fig. 3. The billets were pressed through the thickness, which in combination with the high aspect ratio molding powder provides for an orthotropic microstructure. The specimen notch was cut to have an inclusive angle of 40°, which was subsequently sharpened with a razor blade according to ASTM D5045.

2.2. Experimental method

Fracture toughness measurements were performed using compact tension specimens as defined in ASTM Standard E1820. The geometry was modified to enable a crack opening displacement (COD) gage to be mounted along the loading line, shown in Fig. 4. These specimens were tested using an MTS 880 load frame under constant crosshead displacement rates of 0.025 and 25 mm/s. Load-line displacements were measured with a MTS COD gage 632.03E-31. Tests were performed at −75, −50, −15, 15, 25, 50, and 100 °C using an MTS 612 environmental chamber. The test temperatures were chosen to encompass the three ambient pressure crystalline phases of PTFE (Fig. 1). A single-specimen method for evaluating J-integral values of fracture toughness was elected due to the number of loading conditions of interest. Moreover, loading–unloading methods were avoided due to the visco-elastic nature of PTFE. As a first order approximation of the J-integral failure criterion values were evaluated to

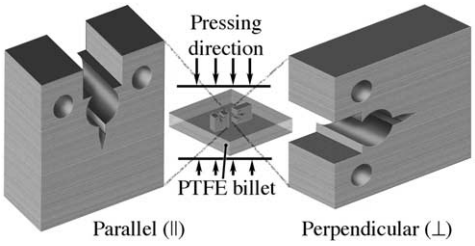

Fig. 3. Compact tension orientation relative to billet pressing direction.

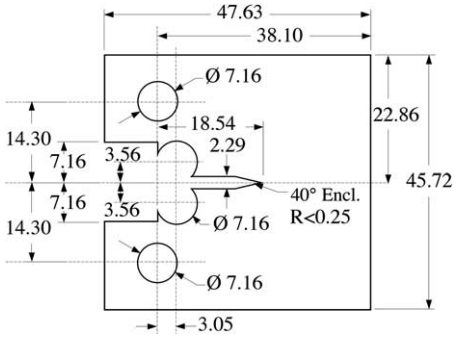

Fig. 4. Compact tension (CT-1/2) fracture specimen geometry with integrated load-line knife-edges for COD gage. (All dimensions in mm).

correspond with the maximum load J_{max}, as proposed by Joyce [17]. J-integral values corresponding to the ith data pair are given by

$$J_i = J_{el_i} + J_{pl_i} = \frac{K_i^2(1-\nu^2)}{E} + \frac{\eta_{pl}A_i^{pl}}{b(w-a_0)}, \quad (1)$$

where J_{el} and J_{pl} signify the division of energy into recoverable elastic deformation and permanent plastic deformation respectively. The Poisson ratio, ν, is taken to be 0.35 as an average from Rae and Brown [25], E is the Young's modulus, $\eta_{pl}=2+0.522(w-a_{bi})/w$ is a dimensionless constant ($a_{bi}=a_0+J_i/2\sigma_{ys}$ is the blunting corrected crack length correspond to the ith data point), A_i^{pl} is the area under the load displacement curve shown in Fig. 5, w and b are the width and the thickness of the specimen, and a_0 is the initial crack length. The linear-elastic stress intensity factor K_i—the stress distribution at the crack tip corresponding to a given far-field load—for a specimen with a crack length of a_i is given by

$$K_i = \frac{P_i}{b\sqrt{w}}\left[\frac{\left(2+\frac{a_0}{w}\right)\left(0.886+4.64\left(\frac{a_0}{w}\right)-13.32\left(\frac{a_0}{w}\right)^2+14.72\left(\frac{a_0}{w}\right)^3-5.6\left(\frac{a_0}{w}\right)^4\right)}{\left(1-\frac{a_0}{w}\right)^{3/2}}\right]. \quad (2)$$

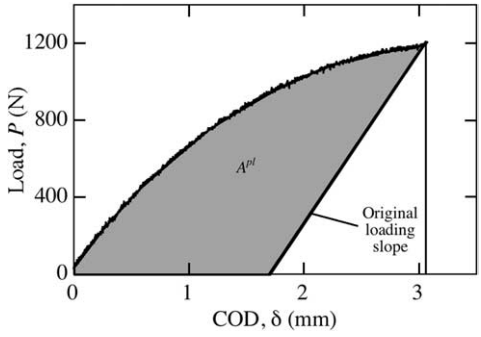

Fig. 5. Representative load-displacement curve. Taken at −15 °C with a loading rate of 0.025 mm/s. Note: the data has been truncated at the data pair corresponding to crack initiation.

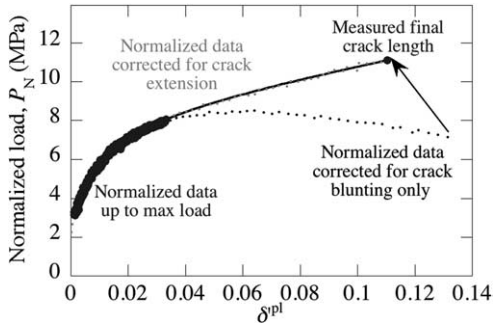

Fig. 6. Representative curve of normalized data. Taken at −15 °C with a loading rate of 0.025 mm/s. For clarity only 5% of data is shown.

For unstable brittle fracture, the peak load (P_{max}) provides a rigorous critical fracture criterion, $J_{max}=J_i(P_i=P_{max})=J_{IC}$. For stable crack propagation, J_{max} generally captures both initiation of crack growth and early propagation, thus over estimating J_{IC}. However, as discussed later, this provides useful insight into orientation dependence of crack behavior.

To rigorously evaluate J_{IC}, J–R curve data are constructed with the critical fracture criterion, J_{IC}, defined as the fracture toughness of the material at fracture instability prior to the onset of significant stable tearing crack extension (the point of 0.2 mm of crack growth beyond crack tip blunting). Due to the wide range of failure behaviors exhibited by PTFE, two methods are employed for measuring crack extension: the normalization technique of the J-integral resistance curve and optical crack tip measurement. The normalization technique was proposed by Landes and Herrera [30] and has been included in ASTM Standard E1820 for elastic-plastic fracture toughness. Although developed for metals, the normalization technique has been demonstrated to yield equivalent results to multi-specimen methods for a variety of polymers [17,18,31–34]. The required data for application of the normalization technique consists of a record of load versus displacement $P_i-\delta_i$, the initial crack length a_0, and the final crack length a_f. The load data P_i up to the maximum load P_{max} is normalized by

$$P_{Ni} = \frac{P_i}{wb\left[\frac{w-a_{bi}}{w}\right]^{\eta_{pl}}}. \quad (3)$$

The final load–displacement data pair is normalized using the final measured crack length a_f. The plastic component of the load-line displacement is normalized as

$$\delta_i' = \frac{\delta_i^{pl}}{w} = \frac{\delta_i - P_i C_i}{w}, \quad (4)$$

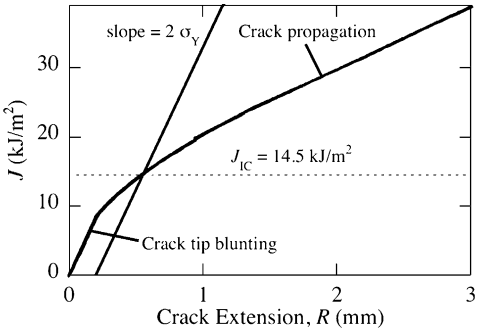

Fig. 7. Representative *J–R* curve obtained using the normalization technique corresponding to −15 °C with a loading rate of 0.025 mm/s.

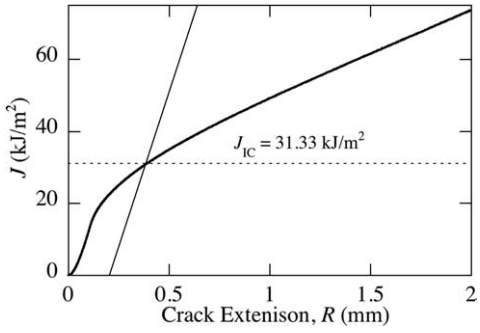

Fig. 9. Representative *J–R* curve obtained using the optical crack tip measurement corresponding to 25 °C with a loading rate of 0.025 mm/s.

where C_i is the specimen elastic load line compliance calculated with the instantaneous crack length,

$$C_i = \frac{1}{Eb}\left(\frac{w+a_i}{w-a_i}\right)^2\left[2.1630 + 12.219\left(\frac{a_i}{w}\right) - 20.065\left(\frac{a_i}{w}\right)^2 - 0.9925\left(\frac{a_i}{w}\right)^3 + 20.609\left(\frac{a_i}{w}\right)^4 - 9.9314\left(\frac{a_i}{w}\right)^5\right]. \quad (5)$$

Prior to crack extension C_i approximates the slope of the load–load line displacement curve. A representative plot of the normalized data set corresponding to the data in Fig. 5 is given in Fig. 6. Normalized data corresponding to $\delta_i' \mathrm{pl} \leq 0.001$ is excluded. The normalized data is fit with a normalization function of the form

$$P_N = \frac{a + b\delta_{pl}' + c\delta_{pl}' 2}{d + \delta_{pl}'}, \quad (6)$$

where a, b, c, and d are fitting coefficients determined with Kaleidagraph (graphical data analysis software from Synergy Software, Reading, PA) while forcing the curve to intercept the final data point. This equation approximates a power law for small δ'_{pl} and smoothly transitions to a linear relationship for large δ'_{pl}. Because crack initiation generally occurs prior to the maximum load in ductile fracture, ASTM standard E1820 requires some manipulation of the normalized data to optimize the fit of the normalization function to the data. Once the normalization function is fixed, the previously excluded data is analyzed by determining the crack length—a value between the blunting corrected crack length and the final crack length—that forces each data pair to fall on the normalization function. These crack lengths give an accurate estimate of the crack tip position over the course of the test. The resulting *J*-integral-crack length data pairs are used to construct a *J–R* curve, shown in Fig. 7, which is subsequently used to determine J_{IC} values. The normalization technique is limited to cases of short crack extension (less than 15% of $w-a$). Moreover, the predicted crack extension from the blunting correction must be small compared to the total measured crack growth. When plasticity and ductile tearing, rather than rigorous crack propagation dominates, the simple model for blunting correction predicts crack extensions that exceed the actual crack extension. In this case, crack extension was measured optically using a digital CCD camera with a macro lens. As shown in Fig. 8(a)–(d), substantial crack tip blunting occurs at room temperature and above, allowing for clear optical measurement of the crack tip location. Crack tip extension was determined by correlating images through time with the initial image through digital image correlation (DIC), as illustrated in Fig. 8(e) by overlaying Fig. 8(a)–(d), to develop a profile of crack extension versus time (Fig. 8(e)).

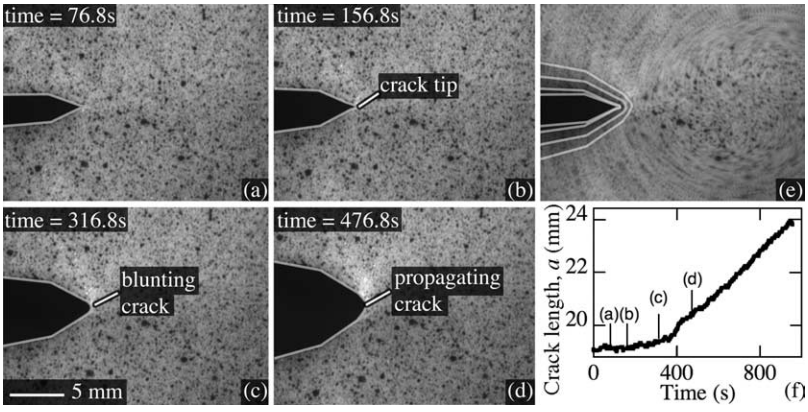

Fig. 8. (a)–(d) Representative images of the crack type development through time at 25 °C with a loading rate of 0.025 mm/s. (e) Correlation of (a)–(d) by DIC to determine crack extension, to determine crack length versus time (f).

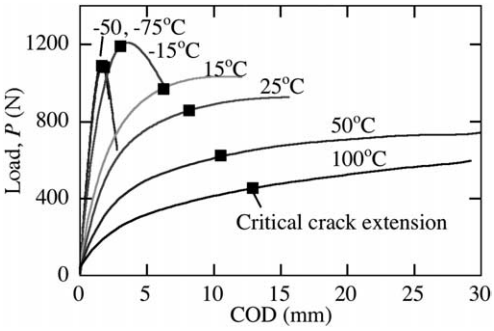

Fig. 10. Representative load–displacement curves at a displacement rate of 0.025 mm/s as a function of temperature for crack growth parallel (||) to the pressing direction. The critical crack extension markers indicate the point of crack growth based on *J–R* curve data.

The resulting *J*-integral-crack length data pairs are used to construct a *J–R* curve, shown in Fig. 9.

2.3. Microscopy

Fracture surface morphologies were examined with a JEOL JSM-6300FXV scanning electron microscope (SEM). After fracture, specimens were notched along the centerline from the backside and subsequently immersed in liquid nitrogen for approximately 30 min. Samples were immediately reloaded to propagate a brittle crack from the arrested crack tip. Areas of interests were then dissected, mounted, and sputtered with carbon to promote electrical conductivity to reduce charging. Micrographs were obtained using 5 keV secondary electrons.

3. Results

Samples of PTFE were tested as a function temperature, rate, and orientation. This section presents the resulting measured load–load-line displacement data and the calculated *J*-integral fracture toughness values. Quasi-static (0.025 mm/s) load–displacement curves for PTFE with crack growth parallel (||) to the pressing direction are shown in Fig. 10 at −75, −50, −15, 15, 25, 50, and 100 °C.

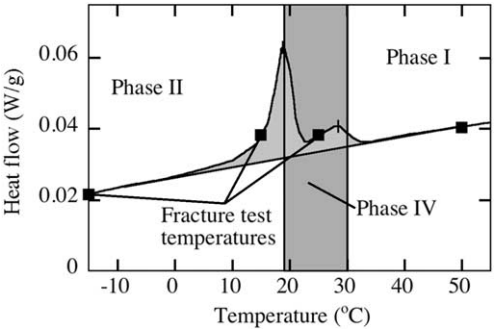

Fig. 11. DSC scan illustrating crystalline phase transitions in relation to test temperatures. Scan performed at 2 °C/min [35].

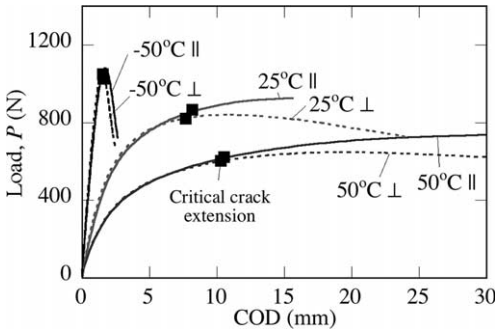

Fig. 12. Representative load–displacement curves as a function of orientation for crack growth parallel (||) to and perpendicular (⊥) to the pressing direction at a displacement rate of 0.025 mm/s. The divergence between the orientations indicates a more rapid drop in load following crack extension. The critical crack extension markers indicate the point of crack growth based on *J–R* curve data.

Samples were soaked at testing temperature for a minimum of one hour to ensure thermal equilibrium. Samples of PTFE tested at −75, −50, and −15 °C have a phase II crystalline structure. Measurement of the heat flow across the 19 and 30 °C phase transitions by differential scanning calorimetry (DSC), as shown in Fig. 11, indicates that below ∼0 °C and above ∼35 °C the heat flow follows that base line indicative of stable crystalline states. The crystalline structure of PTFE at 15 °C is kinetically transitioning from phase II to IV. At 25 °C the crystalline structure of PTFE is phase IV, which converts to phase I at higher temperatures (50 and 100 °C). As expected from the viscoelastic–viscoplastic nature of PTFE 7C reported by Rae and Brown [25] the load-displacement results are non-linear exhibiting compliance increases with temperature. Moreover, it is observed that as the crystalline structure transitions between phases, crack propagation transitions from brittle with stable load drop after crack propagation, to ductile with increasing load during crack propagation. Onset of the phase II to IV transition in PTFE is observed at 15 °C. This coincides with the transition point between brittle and ductile failure in uniaxial tension [25]. It should be noted that calculation of J_{max} assumes the existence of clear peak load (i.e. the load

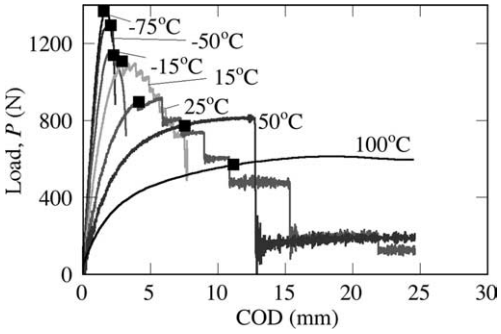

Fig. 13. Representative load–displacement curves at a displacement rate of 25 mm/s, as a function of temperature for crack growth parallel (||) to the pressing direction. The critical crack extension markers indicate the point of crack growth based on *J–R* curve data.

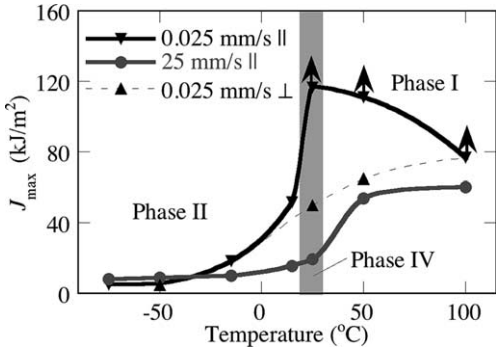

Fig. 14. Strain energy values corresponding to the maximum load, J_{max}, as a function of temperature and rate for crack growth parallel (||) to and perpendicular (⊥) to the pressing direction. Note for crack growth parallel to the pressing direction the load did not reach a maximum value at 25 °C and above, data with an arrow indicate the value of J when the test was stopped. Error bars representing sample-to-sample variability fall within the data points.

increases to a maximum value followed by a decrease associated with propagation of the crack). Since the load-displacement curves at 25 °C and above do not decrease over the range of crack extensions investigated, J_{max} values represent the value of J corresponding with the final data set and represent a lower bound.

The effect of orientation on quasi-static crack behavior is shown in Fig. 12. In each case, prior to crack extension the behavior is independent of orientation. However, following crack propagation the load-displacement curves diverge depending on orientation for each crystalline phase. For PTFE in phase II (at −50 °C), this divergence is simply a more rapid drop in load following crack extension. When PTFE is in phases IV and I, represented by 25 and 50 °C respectively, the load continues to increase following extension for crack growth parallel (||) to the pressing direction, while the load begins to decrease following crack extension for crack growth perpendicular (⊥) to the pressing direction.

Higher rate curves for PTFE at −75, −50, −15, 15, 25, 50, and 100 °C loaded at 25 mm/s are shown in Fig. 13. Similar to the quasi-static fracture data, the load-displacement results are non-linear with compliance increases coupled to temperature. Polytetrafluoroethylene in phase II exhibits similar brittle behavior at both rates (0.025 and 25 mm/s), and similar ductile behavior is observed at both rates for PTFE in phase I. However, a peak load is reached at the faster loading rate. Interestingly, PTFE in phase IV, which exhibits a similar behavior to PTFE in phase I at quasi-static rates, transitions to unstable brittle fracture at the faster loading rate.

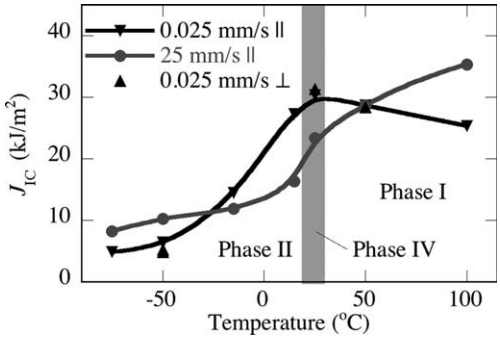

Fig. 15. Fracture toughness values, J_{IC}, as a function of temperature and rate for crack growth parallel (||) to and perpendicular (⊥) to the pressing direction. Error bars representing sample-to-sample variability fall within the data points.

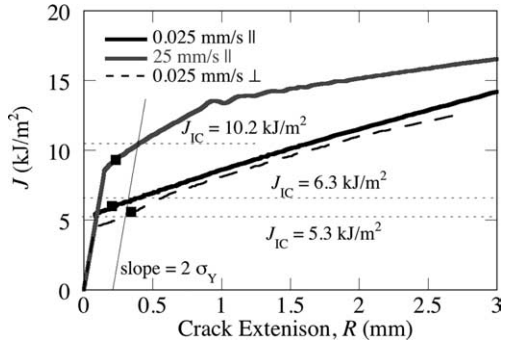

Fig. 16. Representative J–R curves as a function of orientation and rate obtained using the normalization technique corresponding to −50 °C. The data sets corresponding P_{max} are indicated with (■).

Both J_{max} and J_{IC} exhibit a clear transition associated with the crystalline phase transitions, as shown in Figs. 14 and 15. The sample-to-sample repeatability was studied at −50 and 25 °C for both the parallel (||) and perpendicular (⊥) sample orientations. Variation in the measured values of J_{IC} was consistently less then 1%. Both sample orientations at −50 °C and the perpendicular (⊥) samples at 25 °C exhibited variations in J_{max} of less than 1.5%. Since the parallel (||) samples at 25 °C did not exhibit at load drop, the values of J_{max} simply reflects the total elastic and plastic energy put into the sample during the test and sample-to-sample variability was large. However, as a result at 25 °C and above the data points for J_{max} in the parallel (||) samples represent a lower bound, with the presented data representing the highest attained value of J_{max}. At low temperatures (PTFE in phase II), J_{max} exhibits minimal dependence on orientation, with close correlation of J_{max} and J_{IC} values

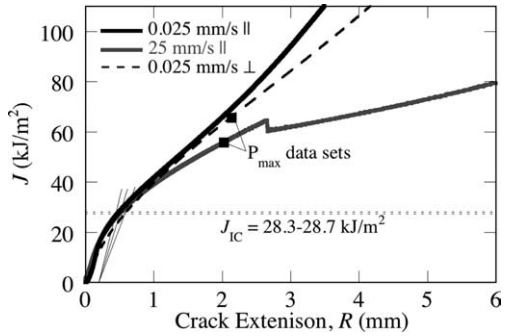

Fig. 17. Representative J–R curves as a function of orientation and rate obtained using the optical crack tip measurement corresponding to 50 °C. The data sets corresponding P_{max} are indicated with (■).

Table 3
Summary of crack behavior dependence on temperature and rate

Crystalline Phase	Phase II			Phase IV		Phase I	
Temperature (°C)	−75	−50	−15	15	25	50	100
Rate (mm/s)	0.025	Brittle with stable crack growth		Ductile with stable crack growth. Crack growth behavior dependent on orientation			
	25			Unstable ductile crack growth			

(Fig. 16). In this regime the *J–R* curves exhibit similar forms independent of rate or orientation, with the crack growth portion of the curve simply shifting to higher values corresponding to J_{IC}. Much higher values of J_{max} are observed for PTFE in phases IV and I (Fig. 17) for crack propagation parallel (∥) to the pressing direction than perpendicular (⊥). The *J–R* curve for the parallel (∥) condition concaves upward, indicating a substantial increase in crack resistance during growth, while the perpendicular (⊥) is nearly linear. Values for the material fracture toughness J_{IC} exhibit nominal dependence on orientation, as shown in Figs. 16 and 17. The temperature and rate dependence is summarized in Table 3.

4. Discussion

4.1. Fractography

Changes in the fracture mechanisms of PTFE associated with crystalline phase transitions are elucidated by investigation of the fracture plane morphology. Two major mechanisms are observed in the scanning electron micrographs: (1) brittle fracture with cleavage fracture surfaces and nominal local deformation representative of microvoid coalescence (as shown in Fig. 18) and (2) ductile failure with significant localized deformation in the form of fibrils (as shown in Figs. 19–21). It should be pointed out that the energy associated with crack propagation in even the brittle failure of PTFE is more than an order of magnitude greater than common structural engineering polymers (see Brown et al. [36] unmodified 828/DETA epoxy $J_{IC} = G_{IC} \cong 0.1$ kJ/m^2, 17 vol% microcapsule modified 828/DETA epoxy $J_{IC} = G_{IC} \cong 0.5$ kJ/m^2). Moreover, the brittle fracture morphology of PTFE exhibits greater similarities to that of metals with a crystalline grain structure (as shown by Powell [37]) than the mirrored morphology of glassy polymers (see for example [36,38]). The primary fibrils formed in the pedigreed PTFE under these conditions are ~1 μm in diameter and can measure up to several mm in length. Some secondary fibrils are observed at domain boundaries during brittle fracture. However, these fibrils are ~10 nm in diameter (including sputtered carbon), i.e. less than 15 aligned PTFE chains, and are limited to micron lengths (Fig. 22).

The onset of fibril formation occurs at 15 °C for quasi-static loading conditions, corresponding to the increased J_{IC} values observed in Fig. 15. In all quasi-static cases where fibrils are observed, the formation process is stable with fibrils occurring over the entire fracture plane. The primary distinction is that only when PTFE is in phase IV are fibrils observed to occur from the immediate point of precrack tip (Fig. 20), while for PTFE transitioning between phases II and IV at 15C (Fig. 19) and for PTFE in phase I (Fig. 21) the

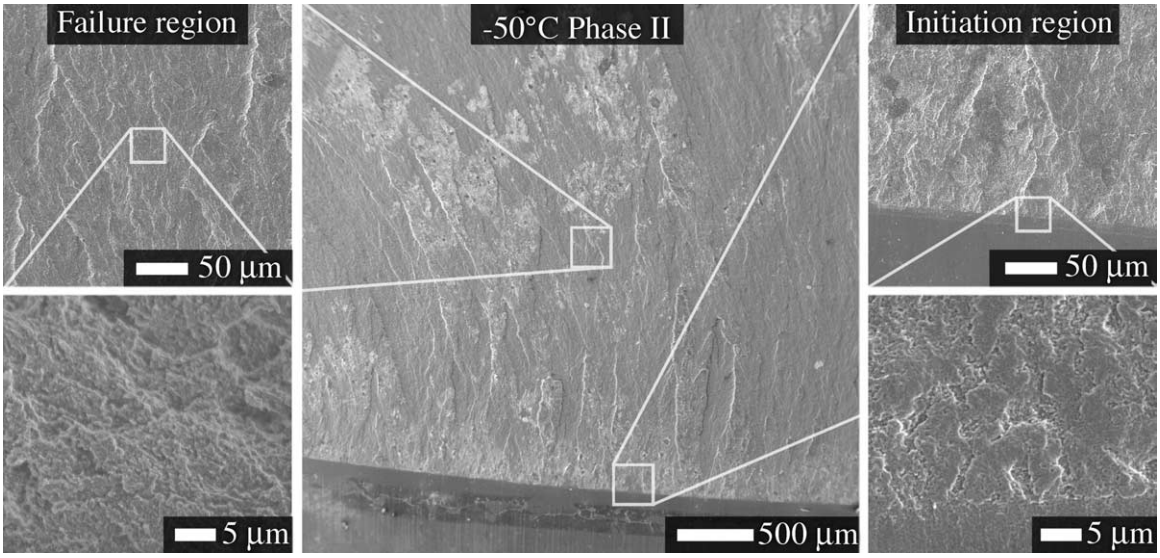

Fig. 18. SEM micrographs of the fracture plane morphology for PTFE 7C in phase II at 0.025 mm/s loading rate. Note: crack propagation is from bottom to top.

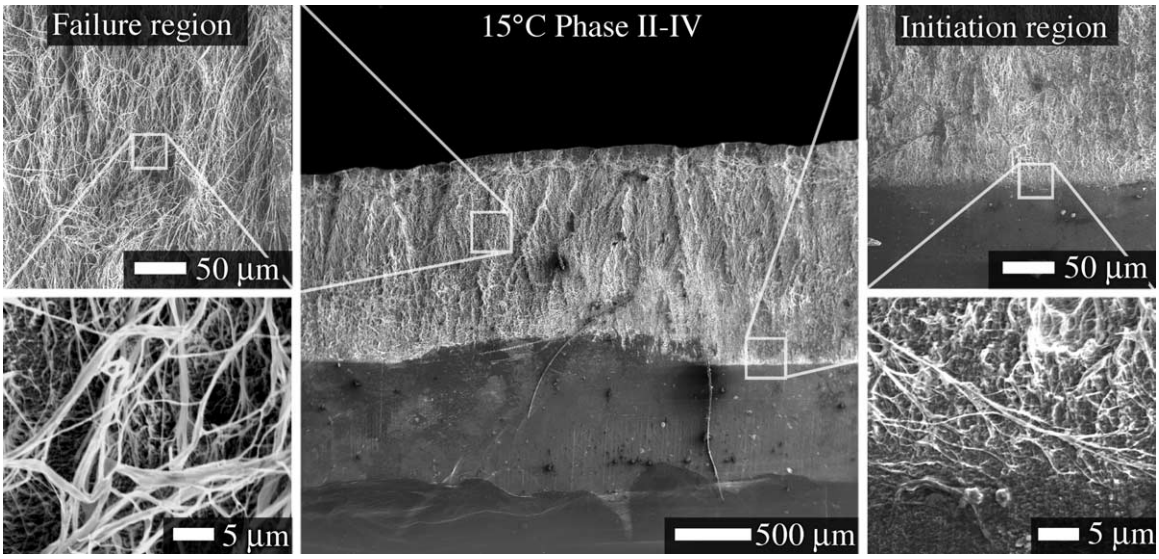

Fig. 19. SEM micrographs of the fracture plane morphology in PTFE 7C during the phase II to phase IV transition at 0.025 mm/s loading rate. Note: crack propagation is from bottom to top.

formation of fibrils near the precrack tip is much less defined.

Fibril formation exhibits a strong dependence on loading rate and orientation. As shown in Fig. 13, at the higher loading rate (25 mm/s) crack propagation occurs in a stick-slip manor. During the period of stable crack growth and arrest, fibrils are formed similar to the quasi-static loading conditions. However, the drawing process is less complete at the higher rate, as shown by the formation of webs between multiple fibrils (Fig. 23), resulting in fibril lock up and ultimately jumping of the crack. The dynamic crack propagation yields regions of brittle fracture morphology. Polytetrafluoroethylene in phase IV, where stick-slip is more prevalent, exhibits a reduction in toughness with rate, while toughness increases with rate at the higher and lower temperatures.

While the initiation of crack propagation exhibits nominal dependence on orientation, the propagation behavior is strongly dependent on orientation. Over the range of temperatures investigated, crack propagation with the crack path perpendicular ($\perp$) to the pressing direction required significantly less energy than parallel ($\parallel$) to the pressing direction. This was indicated by lower values of J_{max} and a clear value of P_{max} followed by a decreasing load. For the case of crack growth parallel ($\parallel$) to the pressing direction, as discussed above, uniform fracture morphologies are observed. When crack growth is perpendicular ($\perp$) to the pressing direction (Fig. 24) and at lower temperatures,

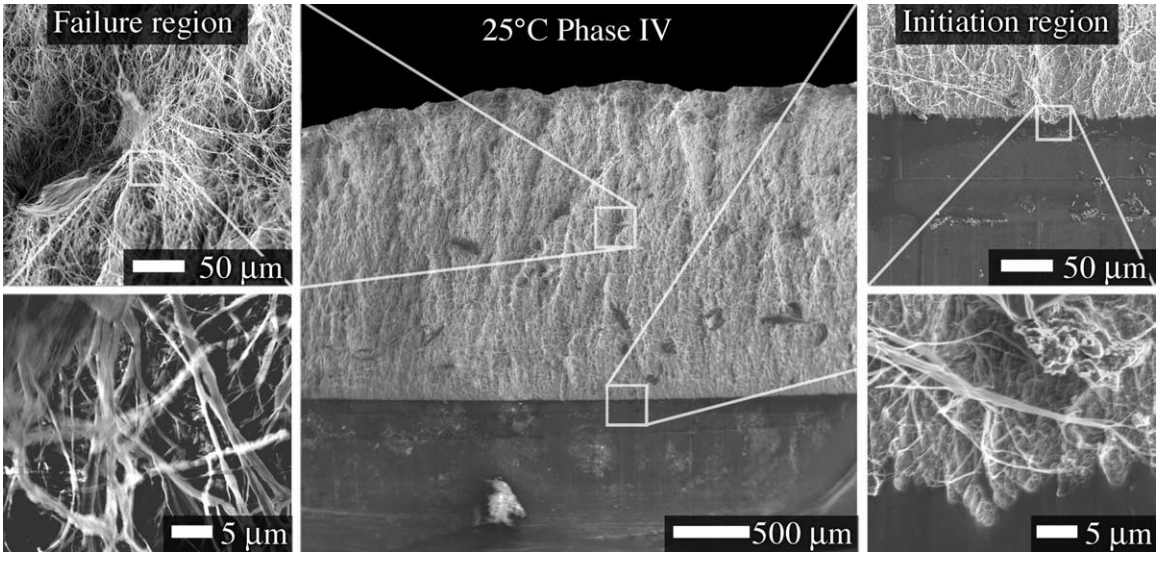

Fig. 20. SEM micrographs of the fracture plane morphology for PTFE 7C in phase IV at 0.025 mm/s loading rate. Note: crack propagation is from bottom to top.

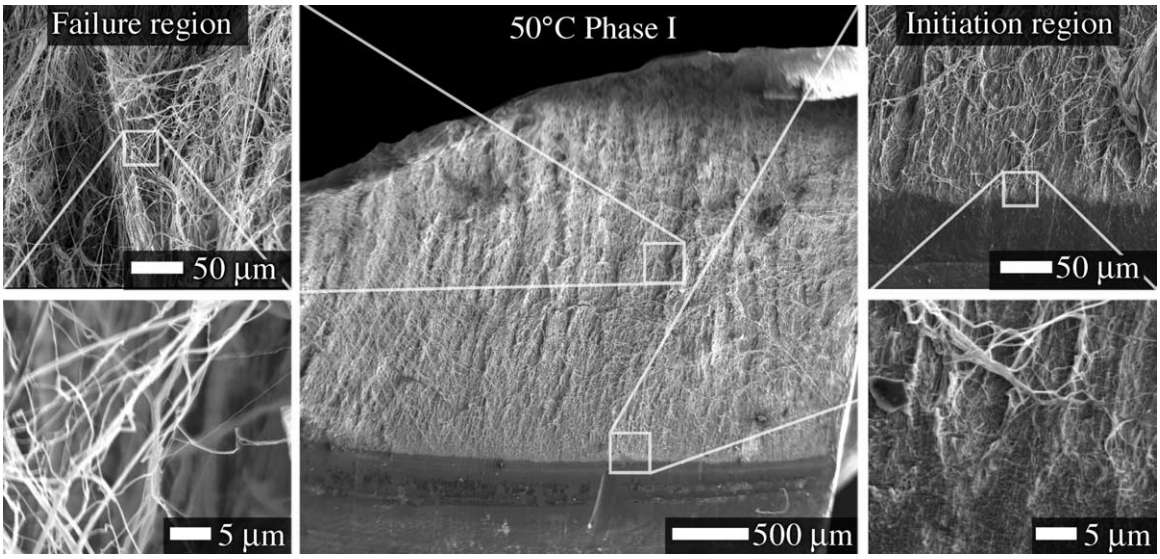

Fig. 21. SEM micrographs of the fracture plane morphology for PTFE 7C in phase I at 0.025 mm/s loading rate. Note: crack propagation is from bottom to top.

brittle fracture is observed, the localized deformation and microvoid coalescence is interspersed with large regions of pure brittle cleavage. At higher temperatures, when fibril formation is observed, the fibrils are less drawn with intermittent regions of fibril formation and microvoid coalescence when crack growth is perpendicular ($\perp$) to the pressing direction (Fig. 25).

4.2. Fibril formation

The stable formation of fibrils in PTFE has received significant interest in the literature. However, this work has not been correlated to damage or fracture. Drawn PTFE films have been used to produce uniform fibril networks to form porous membranes [39,40] and expanded bulk PTFE exhibits a microstructure with a negative Poison ratio [41]. Efforts to improve the formation of uniform fibril networks have shown stable drawing of fibrils can be improved by choice of PTFE prepolymer, polymer processing, elevated temperature (corresponding to PTFE in phase I), and careful application of low rate deformation [39]. However, several contradicting reports on the structure of fibrils have been presented. Kitamura et al. [39] reported that fibril formation is a process of unraveling of the crystalline domains to form an oriented ribbon-like crystalline structure in the direction of loading. O'Leary and Geil [42] measured the structure to be a large perfect, low molecular weight crystal using electron diffraction. Okuyama et al. [43] measure the crystalline structure of individual fibrils using wide angle X-ray line broadening showing the fibril diameter to correspond to the crystalline domain size along the chain axis. Alternately, Ariawan et al. [44] suggest that fibrils are oriented amorphous PTFE formed by unwinding of the crystalline domains. Although the precise structure and formation mechanism of fibrils requires further investigation, estimates of the mechanical strength and stiffness of individual fibrils are consistently greater than the bulk [41,43,44]. Moreover, fibrils nucleate from a point of stress concentration and form in the principle stress direction.

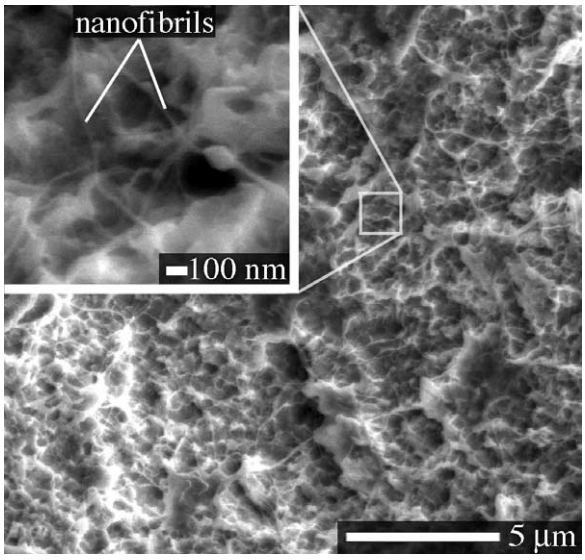

Fig. 22. SEM micrographs of nanofibrils on the fracture plane for PTFE 7C in phase II (−15 °C) at 0.025 mm/s loading rate. Note: crack propagation is from bottom to top.

The ability of polymers other then PTFE to craze and form fibrils in the vicinity of a crack tip has been a topic of intensive study. Fibrils have been shown to provide a mechanism to dissipate energy [45] and stabilize a crack tip by bridging [46,47]. Aglan et al. [26] observed fibrils in reinforced PTFE under fatigue loading conditions and correlated fibril formation with energy dissipation. Joyce alludes to fibril formation in metal-reinforced PTFE [19], but does not report fibril formation in unreinforced PTFE [17,18]. The heterogeneous nature of PTFE arising from crystalline domains in an amorphous matrix provides a

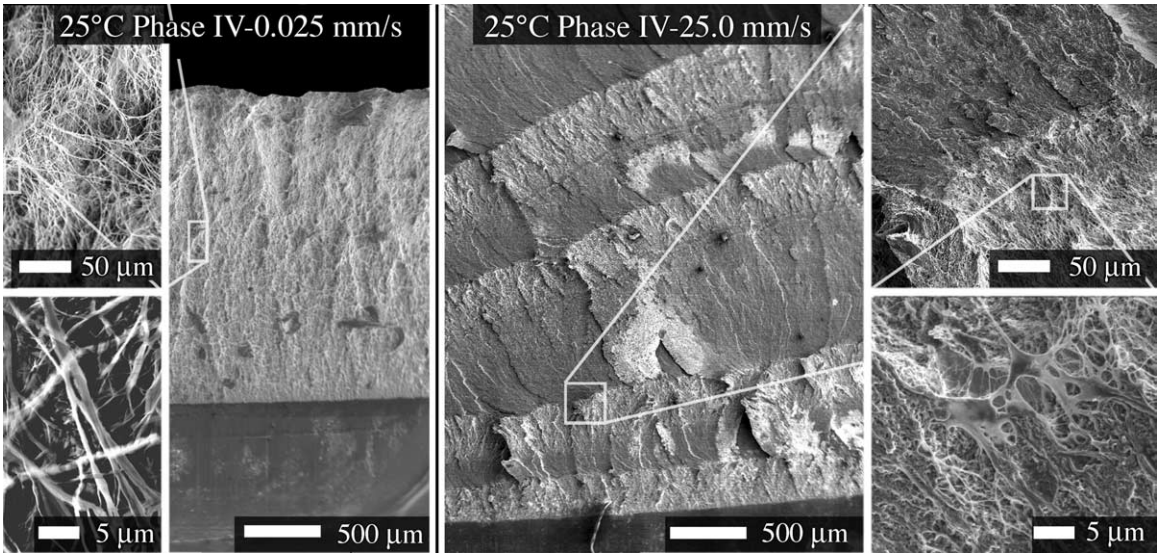

Fig. 23. SEM micrographs of the fracture plane morphology for PTFE 7C in phase IV as a function of rate. Note: crack propagation is from bottom to top.

mechanism for the formation of microvoids in the high stress region near a crack tip, as illustrated in Fig. 26. However, as shown by Wecker et al. [48], the mechanisms by which crystalline domains in PTFE orient themselves under uniaxial loading are dependent on the phase. In the case of PTFE in phase II, there is limited material mobility, and the crystalline domains deform and orient out of the principle stress direction [48]. Here, fracture either occurs as cleavage (Fig. 26(a)) or microvoid coalescence (Fig. 26(b)). This results in brittle crack growth with a low resistance to fracture (low J_{IC}). However, PTFE crystalline domains in phase IV initially deform and orient out of the principle stress direction but rotate into the principle stress direction with additional extension and crystalline domains in phase I preferentially orient into the primary stress direction [48]. Therefore, in the case of PTFE in phase IV or I the material is able to locally deform in the vicinity of microvoids to initiate the stable formation of fibrils. Once initiated, the formation of fibrils is an efficient mechanism to dissipate energy through localized plastic deformation (Fig. 26(c)). Moreover, as the fibrils are drawn, they become increasing strong and stiff. As the fibrils bridge the crack plane, they blunt the crack and shield the material ahead of the crack. The irreversible formation of fibrils provides significant mechanism for plastic deformation of PTFE in phase IV and phase I. Moreover, fibril formation is an orientation process and provides significant increases in the elastic strength of PTFE. The ability of fibrils to bridge the fracture plane provides significant blunting, preventing rapid crack propagation.

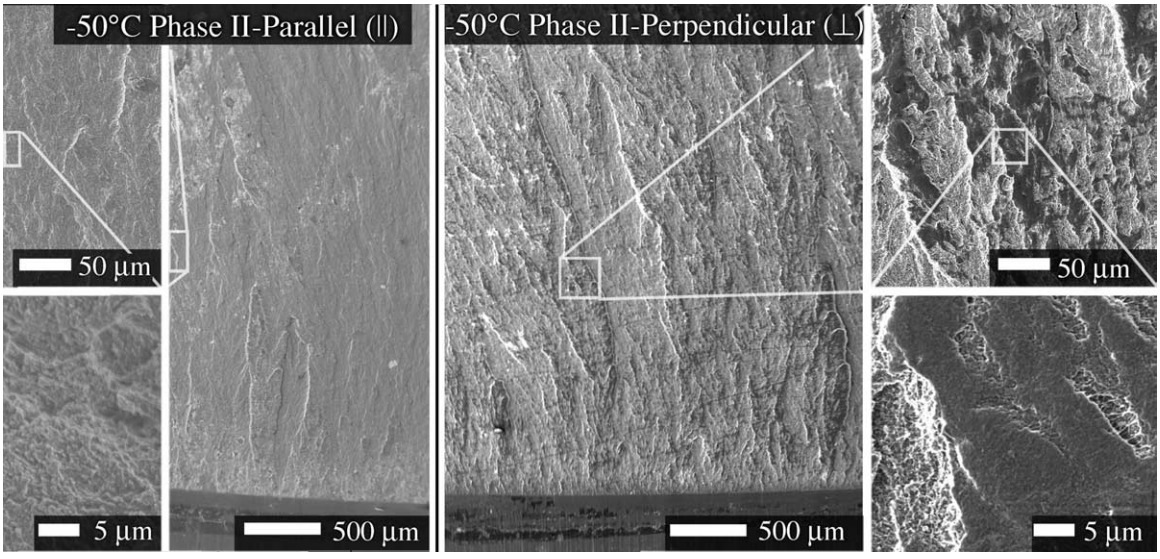

Fig. 24. SEM micrographs of the fracture plane morphology for PTFE 7C in phase II as a function of orientation relative to the pressing direction. Note: crack propagation is from bottom to top.

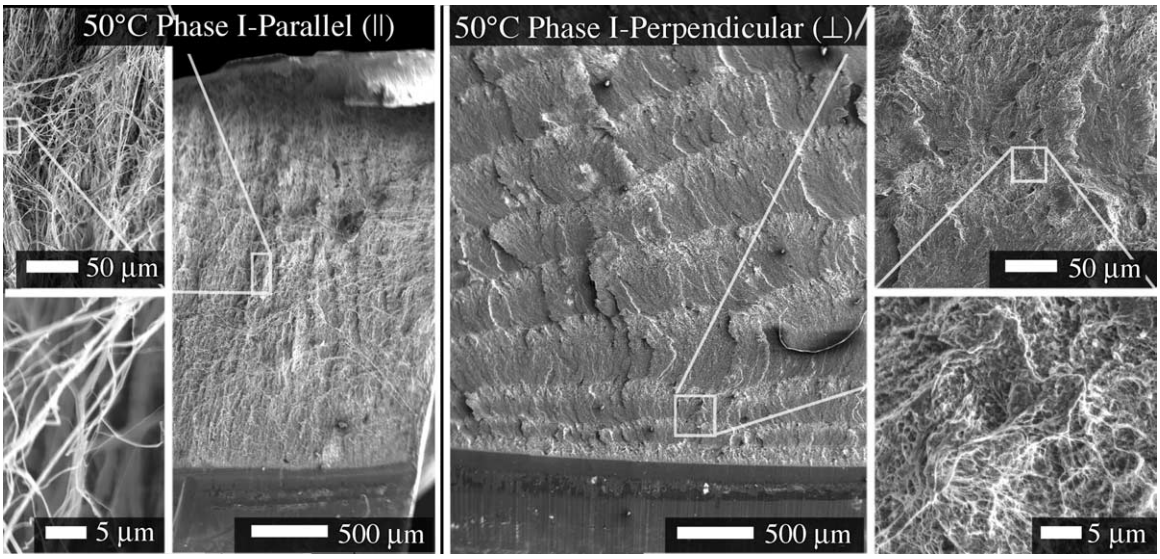

Fig. 25. SEM micrographs of the fracture plane morphology for PTFE 7C in phase I as a function of orientation relative to the pressing direction. Note: crack propagation is from bottom to top.

5. Conclusions

A series of fracture experiments were performed to elucidate the role of crystalline phase on fracture and microstructure evolution in polytetrafluoroethylene (PTFE). Tests were performed over a range of temperatures from −75 to 100 °C capturing the three ambient pressure crystalline structures (phases II, IV, and I) with transitions at 19 and 30 °C. Crack propagation in PTFE is strongly phase dependent with a brittle-to-ductile transition associated with the room temperature phase transitions. The single specimen normalization technique was employed to quantify to the *J*-integral fracture toughness in the brittle phase observed below 19 °C. Above 19 °C extensive crack tip blunting and plastic deformation were observed and crack tip positions were measured optically. Increases in fracture toughness result from the onset of stable fibril formation bridging the crack plane and the increased plastic deformation. The stability of drawing fibrils is primarily determined by temperature and crystalline phase with additional dependence on loading rate and microstructure anisotropy. While fracture toughness values associated with the initiation of crack growth have nominal dependence on orientation, crack propagation perpendicular to the pressing direction is far less stable than when parallel to the pressing direction. This work demonstrates that although PTFE has been considered highly resistant to crack propagation due to its behavior at room temperature, the onset of brittle fracture below room temperature caused by the temperature-induced phase transition necessitates consideration of brittle fracture during service at lowered temperatures.

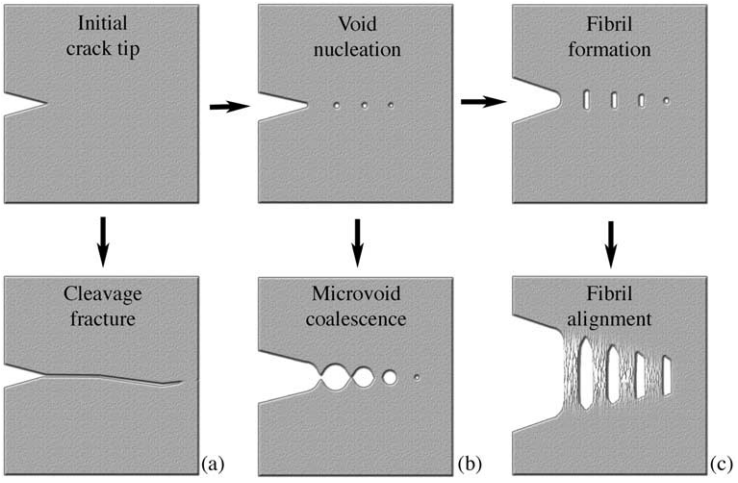

Fig. 26. Schematic of the primary fracture mechanisms observed in PTFE: (a) cleavage, (b) microvoid coalescence, and (c) ductile fibril formation.

Acknowledgements

This research was supported under the auspices of the US Department of Energy operated by the University of California. Specifically, this work was supported, in part, by the joint DOE/DoD Office of Munitions Memorandum of Understanding lead by B. Clements, of the Los Alamos National Laboratory (LANL). E.N. Brown acknowledges the Los Alamos National Laboratory Director's Funded Postdoctoral Fellowship program for support, and the input and guidance of Dr G.T. Gray III. Dr P.J. Rae is thanked for helpful discussions and his aid with mechanical testing. Dr E.B. Orler graciously provided the DSC data. Electron microscopy was performed in the Electron Microscopy Laboratory on a JEOL JSM-6300FXV, MST-8 LANL, with the assistance of Dr R. Dickerson and J. Smith.

References

[1] Sperati CA, Starkweather Jr HW. Fluorine-containing polymers. II. Polytetrafluoroethylene. Advances in polymer science. 2. Berlin: Springer; 1961. p. 465–95.
[2] Cox JM, Wright BA, Wright WW. J Appl Polym Sci 1964;8(6):2935.
[3] Hanford WE, Joyce RM. J Am Chem Soc 1946;68(10):2082.
[4] Gonon P, Sylvestre A. J Appl Phys 2002;92(8):4584.
[5] Briscoe BJ, Ni Z. Wear 1984;100(1–3):221.
[6] Brown EN, Rae PJ, Orler EB, Thissell WR, Dattelbaum DM. Society for Experimental Mechanics X International Congress on Experimental and Applied Mechanics. 2004; 92.
[7] Bunn CW, Howells ER. Nature 1954;174(4429):549.
[8] Clark ES. Polymer 1999;40(16):4659.
[9] Wu CK, Nicol M. Chem Phys Lett 1973;21(1):153.
[10] Sperati CA. Physical constants of poly(tetrafluoroethylene). In: Brandrup J, Immergut GH, editors. Polymer handbook. 2nd ed. New York: Wiley; 1975. p. V29–V36.
[11] Bunn CW, Cobbold AJ, Palmer RP. J Polym Sci 1958;28(117):365.
[12] Weeks JJ, Sanchez IC, Eby RK, Poser CJ. Polymer 1980;21(3):325.
[13] Williams JG, Hodgkinson JM. Proc R Soc Lond A 1981;375(1761):231.
[14] Khan A, Zhang HY. Int J Plast 2001;17(9):1167.
[15] Fischer S, Brown N. J Appl Phys 1973;44(10):4322.
[16] Zerilli FJ, Armstrong RW. AIP Conf Proc 2002;620(1):657.
[17] Joyce JA. Polym Engng Sci 2003;43(10):1702.
[18] Joyce PJ, Joyce JA. Int J Fract 2004;127(4):361.
[19] Joyce JA, Joyce PJ. Engng Fract Mech 2004;71(16–17):2513.
[20] McCrum NG. J Polym Sci 1959;34(127):355.
[21] Vincent PI. Polymer 1974;15(2):111.
[22] Kisbenyi M, Birch MW, Hodgkinson JM, Williams JG. Polymer 1979;20(10):1289.
[23] Hu TY. Wear 1982;82(3):369.
[24] Dattelbaum DM, Orler EB, Brown EN. Unpublished results 2004.
[25] Rae PJ, Brown EN. Submitted for publication.
[26] Aglan H, Gan Y, El-Hadeki M, Faughnan P, Bryan C. J Mater Sci 1999;34(1):83.
[27] Dupont. Teflon® PTFE 7C, Fluoropolymer resin product information sheet 1999.
[28] Rae PJ, Dattelbaum DM. Polymer 2004;45(22):7615.
[29] Lehnert RJ, Hendra PJ, Everall N, Clayden NJ. Polymer 1997;38(7):1521.
[30] Landes JD, Herrera R. Int J Fract 1988;36(1):R9.
[31] Bernal CR, Montemartini PE, Frontini PM. J Polym Sci 1996;34(11):1869.
[32] Che M, Grellman W, Seidler S, Landes JD. Fatig Fract Engng Mater 1997;20(2):119.
[33] Morhain C, Velasco JI. J Mater Sci 2001;36(6):1487.
[34] Landes JD, Bhambri SK, Lee K. J Test Eval 2003;31(2):1.
[35] Orler EB. Personal communication 2004.
[36] Brown EN, White SR, Sottos NR. J Mater Sci 2004;35(5):1703.
[37] Powell GW. Mater Characterization 1994;33(3):275.
[38] Kusy RP, Turner DT. Polymer 1977;18(4):391.
[39] Kitamura T, Okabe S, Tanigaki M, Kurumada K, Ohshima M, Zanazawa S. Polym Engng Sci 2000;40(3):809.
[40] Hommura S, Kunisa Y, Terada I, Yoshitake M. J Fluorine Chem 2003;120(2):151.
[41] Alderson A, Evans KE. J Mater Sci 1995;30(13):3319.
[42] O'Leary K, Geil PH. J Appl Phys 1967;38(11):4169.
[43] Okuyama H, Kanamoto T, Porter RS. J Mater Sci 1994;29(24):6485.
[44] Araiwan AB, Ebnesajjad S, Hatzikiriakos SG. Polym Engng Sci 2002;42(6):1247.
[45] Jie M, Tang CY, Li YP, Li CC. Theor Appl Fract Mech 1998;28(3):165.
[46] Sun BN, Hsiao CC. J Appl Phys 1985;57(2):170–4.
[47] Marissen R. Polymer 2000;41(3):1119.
[48] Wecker SM, Davidson T, Baker DW. J Appl Phys 1972;43(11):4344.